GSA Data Repository 2016280

Extensive Noachian fluvial systems in Arabia Terra: Implications for early martian climate

Supplementary Material

J. M. Davis, M. Balme, P. M. Grindrod, R. M. E. Williams, S. Gupta

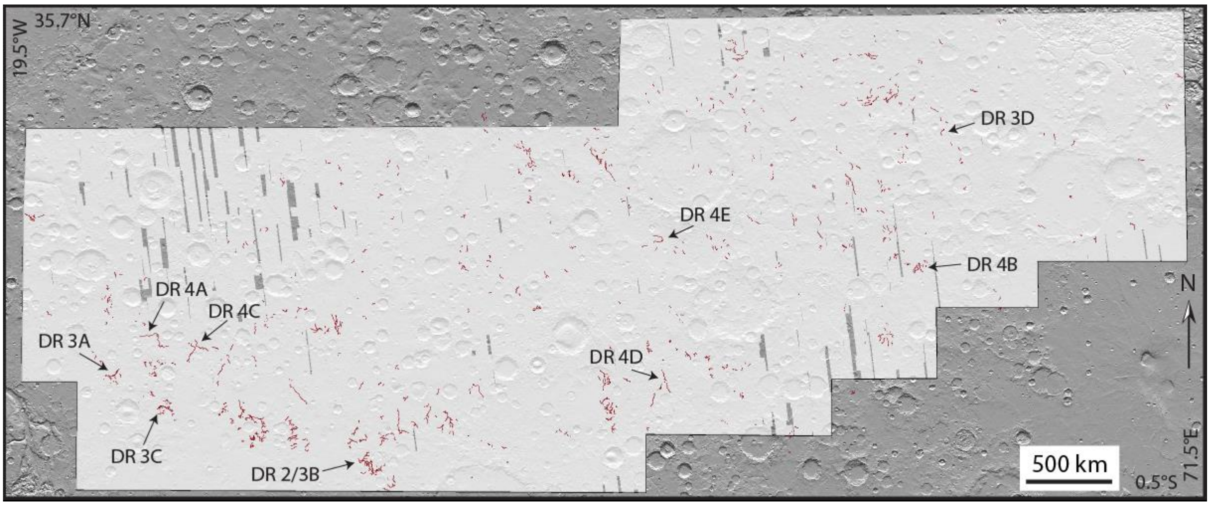

Figure DR 1: Mars Reconnaissance Orbiter (MRO) Context Camera (CTX; 6 m/pixel; Malin et al., 2007) coverage of study area in Arabia Terra. The white shaded area shows the CTX image footprints that were examined, where the image coverage is near 100%. Inverted channels are shown in red. Context locations are also shown for all supplementary figures.

Total observed channel length (from CTX data; ~ 6 m/pixel)	~17,400 km
Highest stream order	7
Longest continuous segment	~200 km
Maximum channel width	~1500 m
Maximum channel height above surrounding terrain	~60 m
Minimum channel elevation	~ -2400 m
Maximum channel elevation	~ +1250 m

Table DR 1: Summary table of Arabia Terra inverted channel characteristics.

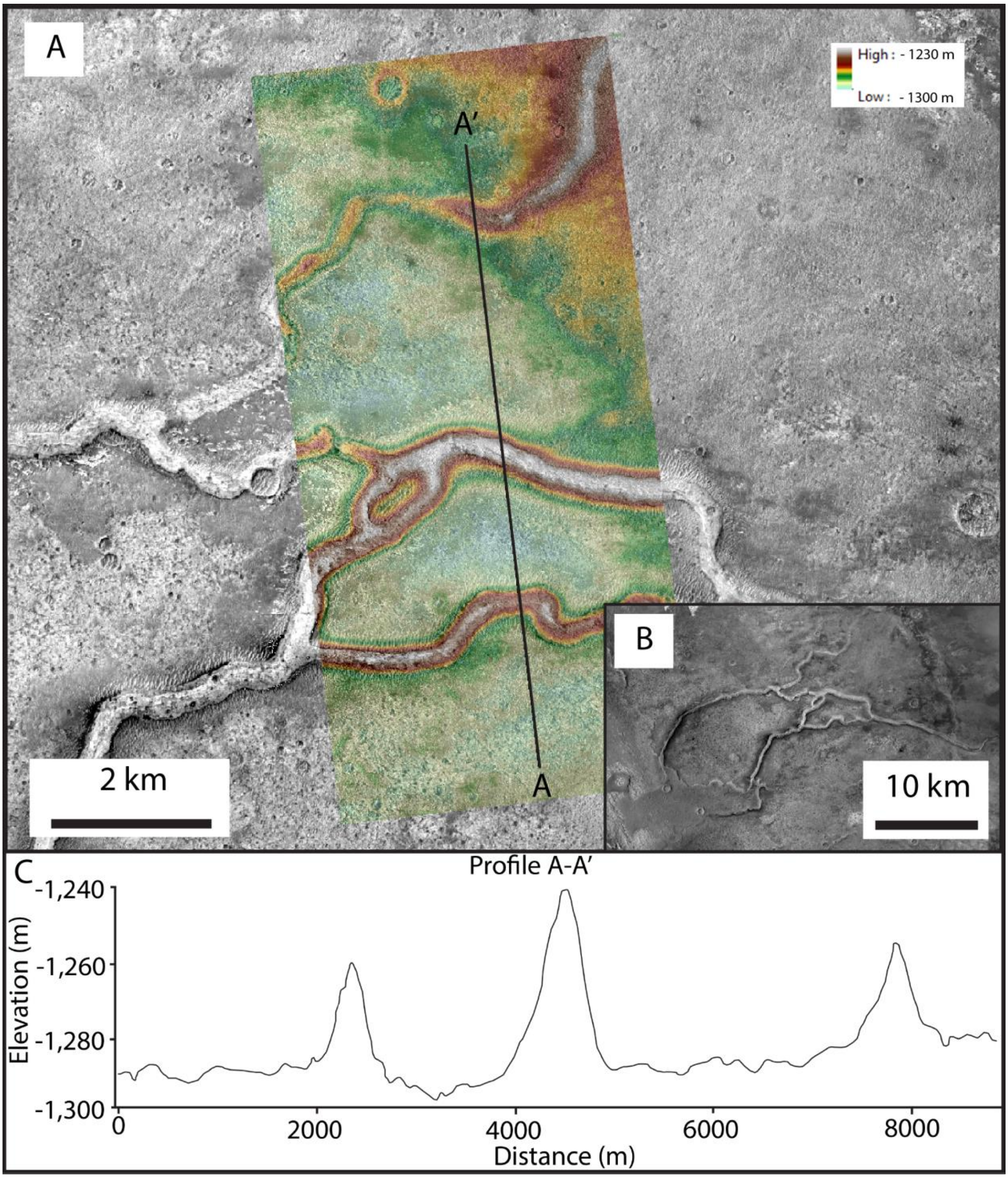

Figure DR 2: (A) MRO High Resolution Imaging Science Experiment (HiRISE; ~25 cm/pixel; McEwen et al., 2007) resolution digital elevation model (DEM; ~1 m/pixel) showing an inverted channel system. The DEM was produced according to the method of Kirk et al. (2008). (B) CTX image mosaic for this inverted channel system. (C) Topographic profile (A-A') of the inverted channel system extracted from HiRISE DEM above. The inverted channels here are up to ~60 m high and almost 1 km in width. Elsewhere, inverted channels are typically ~10-60 m high. However, these values do not represent former channel depth, but instead give an indication of the minimum thickness of marginal alluvium that was removed prior to etched unit emplacement. Assuming the channels were emplaced and fully inverted between the mid- to late Noachian, a period of 200 Ma, the average erosion rate was therefore ~50-300 nm/yr. This is comparable to the low end of values previously estimated for erosion rates during the mid- to late Noachian (~100s to 1000s of nm/yr; Golombek et al., 2006).

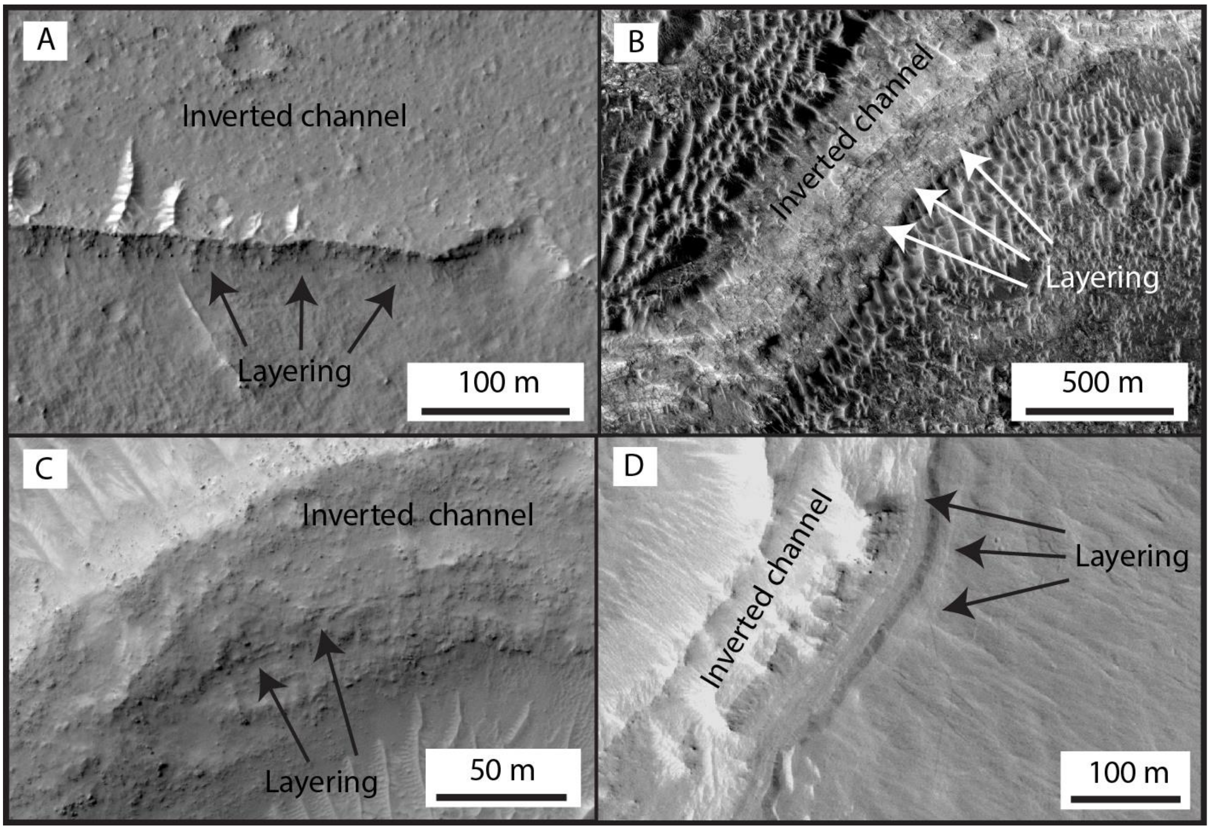

Figure DR 3: HiRISE images show sub-horizontal meter to decameter-scale internal layering exposed at the edges of inverted channels, throughout Arabia Terra. The layering is consistent with the inverted channels being composed of indurated channel floor sediment.

Figure DR 4 (*overleaf*)**:** Inverted channels systems across Arabia Terra; (A) Near continuous inverted channel in the east becomes more segmented towards the west, where it is nearly level with the adjacent material; (B) Branching and sinuous inverted channels which terminate in an infilled crater, which could be an exhumed paleolake deposit, or alternatively, infilling etched material; see also Fassett and Head, 2007, Grant and Schultz, 1990; (C) Inverted channel with possible capping unit; (D and E) Distal ends of Naktong and Scamander Valles, respectively, where inverted channels are present within the negative relief valley networks.

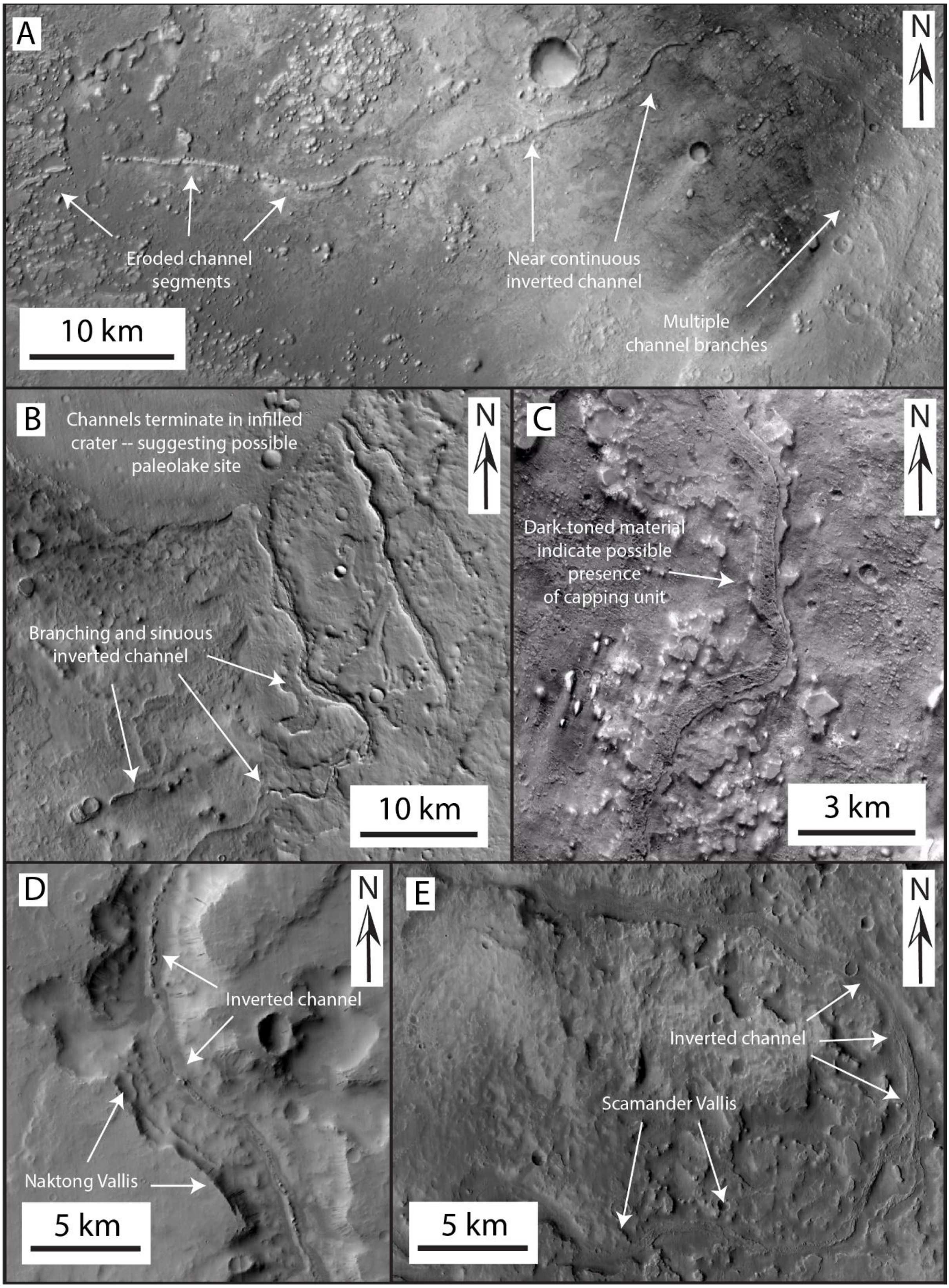
A
N
Eroded channel segments
Near continuous inverted channel
Multiple channel branches
10 km
B
Channels terminate in infilled crater -- suggesting possible paleolake site
N
Branching and sinuous inverted channel
10 km
C
N
Dark-toned material indicate possible presence of capping unit
3 km
D
N
Inverted channel
Naktong Vallis
5 km
E
N
Inverted channel
Scamander Vallis
5 km

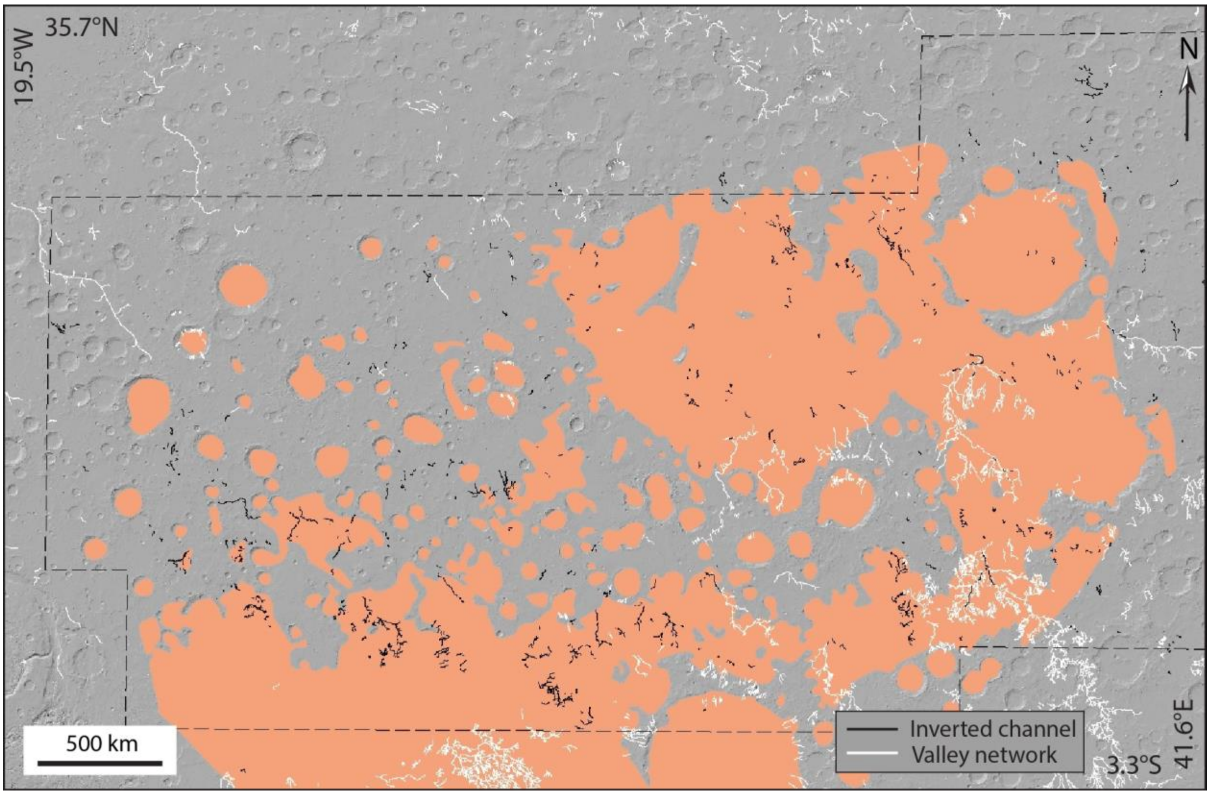

Figure DR 5: Paleo-surface showing former extent of etched units (orange) by Zabrusky et al. (2012; Figure 9, surface a) overlaid on MOLA hillshade map of western Arabia Terra. ~80% of inverted channels (solid black lines) are spatially associated with this surface, suggesting that the etched units have protected the inverted channels from erosion. Adapted from Zabrusky et al. (2012).

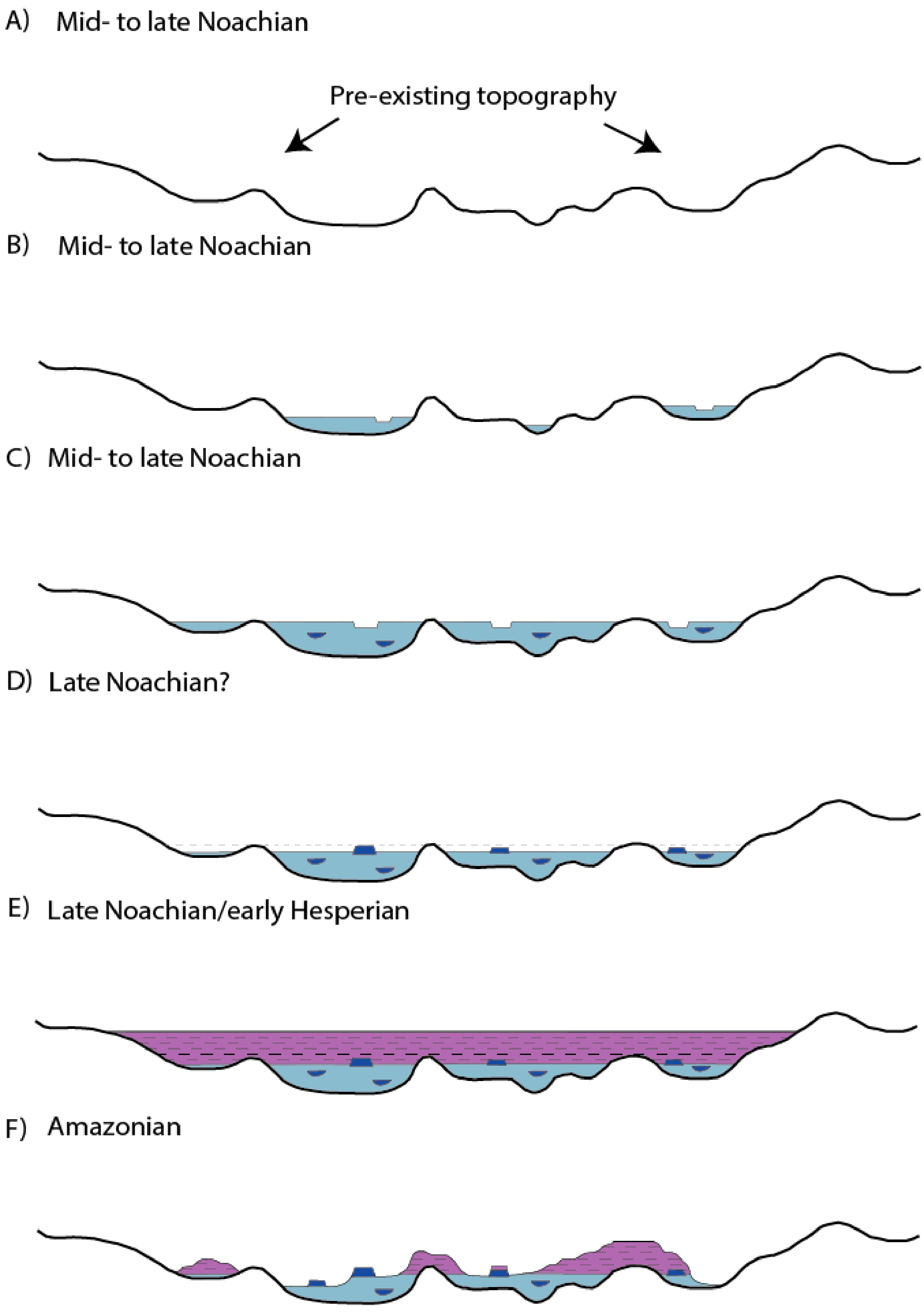

Figure DR 6: Possible sequence of inverted channel formation; A) Pre-existing topography; B) Sediment deposition in topographic lows, possibly in isolated alluvial plains, and formation of discrete fluvial channels; C) Continued aggradation, merging of smaller alluvial systems, and burial of older channels; D) Waning of fluvial activity, ongoing eolian abrasion leaves indurated channel sediment preserved in positive relief; E) Burial and protection of inverted channels by etched units; F) Regional deflation removes etched units and exposes inverted channels to the surface environment.

Figure	Instrument	Image ID
Fig. 1	MOLA*	Global mosaic derived product
Fig. 2A	CTX	B03_010829_1892_XI_09N012W; B01_009840_1885_XN_08N010W; D09_030714_1876_XI_07N011W; G23_027180_1889_XI_08N011W
Fig. 2B	CTX	B10_013532_1835_XN_03N006W; D04_028881_1843_XI_04N007W; B03_010697_1875_XI_07N007W
Fig. 3A	THEMIS nighttime**	Global mosaic derived product
Fig. 3B	HiRISE	PSP_004091_1845
Fig. 4	CTX	B19_017012_1877_XN_07N333W; D01_027627_1876_XI_07N333W
Fig. DR 1	MOLA (hillshade)	Global mosaic derived product
Fig. DR 2A	CTX and HiRISE	ESP_012714_1815; ESP_012714_1815; P04_002627_1808_XN_00N352W; G23_027298_1822_XI_02N352W
Fig. DR 2B	CTX	P04_002627_1808_XN_00N352W; G23_027298_1822_XI_02N352W; P07_003616_1815_XI_01N353W
Fig. DR 3A	HiRISE	ESP_036384_1880
Fig. DR 3B	HiRISE	ESP_012648_1815
Fig. DR 3C	HiRISE	ESP_033586_2065
Fig. DR 3D	HiRISE	ESP_022221_1850
Fig. DR 4A	CTX	P22_009774_1916_XN_11N009W; B17_016143_1909_XI_10N008W; B17_016288_1919_XN_11N008W; B06_011831_1914_XN_11N008W
Fig. DR 4B	CTX	P07_003588_1958_XN_15N310W; P03_002032_1959_XN_15N310W
Fig. DR 4C	CTX	P18_008139_1900_XN_10N004W; P09_004023_1915
Fig. DR 4D	CTX	P19_008375_1874_XN_07N329W
Fig. DR 4E	CTX	P15_006872_1983_XI_18N329W; P13_006160_1977_XN_17N330W
Fig. DR 5	MOLA (hillshade)	Global mosaic derived product

Table DR 2: Instrument and image ID numbers used in all figures.

*Smith et al., 2001

**Christensen et al., 2004

References:

Christensen, P.R., et al., 2004, The Thermal Emission Imaging System (THEMIS) for the Mars 2001 Odyssey mission: Space Science Reviews, v. 110, p. 85–130, doi: 10.1023 /B:SPAC.0000021008.16305.94.

Fassett, C.I., and Head, J.W., III, 2007, Layered mantling deposits in northeast Arabia Terra, Mars: Noachian-Hesperian sedimentation, erosion, and terrain inversion: Journal of Geophysical Research, v. 112, E08002, doi: 10.1029/2006JE002875.

Golombek, M.P., et al., 2006, Erosion rates at the Mars Exploration Rover landing sites and long-term climate change on Mars: Journal of Geophysical Research, v. 111, E12S10, doi: 10.1029/2006JE002754.

Grant, J.A., and Schultz, P.H., 1990, Gradational epochs on Mars: Evidence from West-Northwest of Isidis Basin and Electris: Icarus, v. 84, p. 166-195, doi: 10.1016/0019-1035(90)90164-5.

Hynek, B.M., Beach, M., and Hoke, M.R.T., 2010, Updated global map of Martian valley networks and implications for climate and hydrologic processes: Journal of Geophysical Research, v. 115, E09008, doi: 10.1029/2009JE003548.

Kirk, R.L., et al., 2008, Ultrahigh resolution topographic mapping of Mars with MRO HiRISE stereo images: Meter-scale slopes of candidate Phoenix landing sites: Journal of Geophysical Research, v. 113, E00A24, doi: 10.1029/2007JE003000.

Malin, M.C., et al., 2007, Context Camera Investigation on board the Mars Reconnaissance Orbiter: Journal of Geophysical Research, v. 112, E05S04, doi: 10.1029/2006JE002808.

McEwen, A.S., et al., 2007, Mars Reconnaissance Orbiter's High Resolution Imaging Science Experiment (HiRISE): Journal of Geophysical Research, v. 112, E05S02, doi: 10.1029/2005JE002605.

Smith, D.E., et al., 2001, Mars Orbiter Laser Altimeter: Experiment summary after the first year of global mapping of Mars: Journal of Geophysical Research, v. 106, p. 23,689–23,722, doi: 10 .1029/2000JE001364.

Zabrusky, K., Andrews-Hanna, J.C., and Wiseman, S.M., 2012, Reconstructing the distribution and depositional history of the sedimentary deposits of Arabia Terra, Mars: Icarus, v. 220, p. 311–330, doi: 10.1016/j.icarus.2012.05.007.